





Neutron Tunneling: A New Mechanism to Power Explosive Phenomena in Neutron Stars, Magnetars, and Neutron Star Mergers

Carlos A. Bertulani  and Ronaldo V. Lobato Department of Physics and Astronomy, Texas A&M University-Commerce, Commerce, TX 75429, USA; carlos.bertulani@tamuc.edu, ronaldo.lobato@tamuc.edu*Received 2020 November 27; revised 2021 March 19; accepted 2021 March 22; published 2021 May 11*

Abstract

Neutron tunneling between neutron-rich nuclei in inhomogeneous dense matter encountered in neutron star crusts can release enormous energy on a short timescale to power explosive phenomena in neutron stars. In this work, we clarify aspects of this process that can occur in the outer regions of neutron stars when oscillations or cataclysmic events increase the ambient density. We use a time-dependent Hartree–Fock–Bogoliubov formalism to determine the rate of neutron diffusion and find that large amounts of energy can be released rapidly. The roles of nuclear binding, two-body interaction, and pairing in neutron diffusion times are investigated. We consider a one-dimensional quantum diffusion model and extend our analysis to study the impact of diffusion in three dimensions. We find that these novel neutron transfer reactions can generate energy in the amount of $\simeq 10^{40}$ – 10^{44} erg under suitable conditions and assumptions.

Unified Astronomy Thesaurus concepts: [Neutron stars \(1108\)](#); [Soft gamma-ray repeaters \(1471\)](#); [Gamma-ray sources \(633\)](#)

1. Introduction

The physics of neutron stars and the role played by the details of strongly interacting many-body systems have been a major area of research in astrophysics, based on a limited number of astronomical observations that motivated the development of numerous theoretical models (for reviews, see, e.g., Baym & Pethick 1979; Heiselberg & Pandharipande 2000; Lattimer & Prakash 2004; Chamel & Haensel 2008; Baym et al. 2018). In particular, the physics of neutron star crusts has attracted the interest of an increasing number of nuclear theorists because of, among other phenomena, the prediction of complex structures arising from the interactions between nucleons and electrons (see, e.g., Blaschke et al. 2008; Chamel & Haensel 2008; Bertulani & Piekarewicz 2012). Isospin imbalance occurs in the crust of neutron stars where dense neutron regions coexist with neutron-poorer regions. However, unless disrupting phenomena take place, the crust is rather energetically balanced, and little or no isospin transfer is expected. If isospin together with energy imbalance is established, the relaxation times leading to equilibrium are very short due to beta-decay processes, but neutron tunneling between nuclei has also been suggested as a probable reason for fast equilibration in the environment of white dwarfs (Saakyan & Sedrakyan 1972). Similar considerations have been made for neutron tunneling in the crust of neutron stars. In the inner crust, above the neutron drip density of $\sim 4 \times 10^{11}$ g cm $^{-3}$, a neutron gas of unbound neutrons exists with all bound states occupied, thus leading to isospin equilibration by diffusion of unbound neutrons (see, e.g., Bisnovaty-Kogan & Chechetkin 1979). In the outer crust, neutron transfer between accreted nuclei has been studied with the prediction that they modify the cooling rates in transiently accreting neutron stars (Chugunov 2018, 2019).

A fracture of the crust in a highly magnetized neutron star can reshuffle the magnetic field of the star. A sudden reorganization of the magnetic field may also be the cause of a crack in the surface. In either situation, the quick release of stored energy can occur via powerful bursts that can vibrate the

crust and crack it into pieces that move away from each other, a motion that might be imprinted on gamma-ray bursts and on X-ray signals (Pacini & Ruderman 1974; Blaes et al. 1989; Huppenkothen et al. 2014). The breaking strain of the crust by tidal forces or by resonant elastic modes has also been proposed to generate precursor flares prior to short gamma-ray bursts due to phase transitions of the lattice, as shown in some theoretical models (Troja et al. 2010; Tsang et al. 2012; Chamel 2013). In Kobyakov & Pethick (2014), it was shown that even slight modifications of local neutron densities in the crust above the neutron drip density can give rise to an attractive interaction between the nuclei via interstitial neutrons in a lattice formed by nuclei and electrons. This mechanism likely leads to agglutination of nuclei in a form similar to the formation of inhomogeneous regions in metallic alloys, also known as spinodal decomposition (Kobyakov & Pethick 2014). Huge energy releases, of the order of $\gtrsim 10^{40}$ erg, are expected to be generated in such cataclysmic scenarios, perhaps being responsible for phenomena such as bursts/flaring in soft gamma-ray repeaters (SGRs) and in anomalous X-ray pulsars (AXPs; SGRs/AXPs are commonly called magnetars), as well as fast radio bursts (FRBs).

The outer crust of a neutron star is composed of a lattice of nuclei in a gas of moving electrons. As one goes deeper into the inner crust, the nuclei become more neutron rich, up to a point where neutrons start dripping out of the nuclei. Even deeper in the crust, nuclear clusters with exotic shapes will form, due to a competition between the nuclear and Coulomb interactions (Ravenhall et al. 1983). This neutron-rich system is in energetic equilibrium, but the rupture of the neutron star crust by tidal forces, resonant elastic modes, or magnetic field reshuffling can fuel the formation of a different kind of inhomogeneous neutron distribution (defects in the crystalline structure, Kondratyev 2002, or impurities, which are represented by nuclei whose value of mass or charge (A_i , Z_i) differs from the nuclei of the background, De Blasio & Lazzari 1998) away from energy equilibrium, allowing for the sudden diffusion of neutrons by tunneling between the neutron-rich region to the

region poorer in neutrons, quickly lowering the energy of the system. A fast homogenization of the neutron density ensues with a large release of energy. We explore if this mechanism could be responsible for bursts in SGRs/AXPs and FRBs. Our study is also important in other astrophysical scenarios, e.g., neutron transfer or diffusion in neutron star mergers can also influence the rate at which a locally homogeneous density can be achieved. Deformed neutron-rich lattices and gaps are certainly formed during the merging process and/or during a fallback mechanism in core-collapse supernovae. Supernova fallback accretion has been intensively studied as a possible site for r -process (Fryer et al. 2006) and as a source of long-duration gamma-ray bursts in newly formed magnetars (Piro & Ott 2011; Metzger et al. 2018). We explore the physics of diffusion by tunneling in inhomogeneous neutron media considering the flow of individual neutrons as well as neutron pairs through the nuclear mean field. For simplicity, we assume charge-neutral systems, i.e., pure neutron matter. Our goal is to identify general features and possible scaling laws for the diffusion rates that can be used to estimate diffusion rates important for cooling properties of neutron stars, and relaxation times.

The neutron-rich impurities considered in this work are not typical neutron-rich nuclei accreted at the surface of neutron stars, like those considered in Chugunov (2019). Within the neutron star crust, and in particular, in the inner crust, the proton fraction is expected to be very small, with the formation of complex and large neutron-rich structures, e.g., identified in semiclassical Monte-Carlo simulations (Piekarewicz & Sánchez 2012). A long-accepted idea is that large and strange-looking neutron-rich nuclei, such as “pasta nuclei,” can be formed within the crust (Ravenhall et al. 1983). It has also been shown that such structures might not exist and that their formation strongly depends on the symmetry energy part of the equation of state of nuclear matter (Oyamatsu & Iida 2007). However, with or without pasta nuclei, there is consensus in the literature that very neutron-rich structures are part of the neutron star crust (see e.g., Figure 3 of Piekarewicz & Sánchez 2012). Such structures are believed to be immersed within a low-density electron and neutron gas. In energetic equilibrium, the neutrons within those regions are confined due to their increased mutual interactions and do not diffuse to other neighboring regions. Assuming that a cataclysmic event can deform the lattice that composes the crust, disrupting the neutron distribution, which leads to neutron tunneling between neutron-rich regions and to neutron gaps, we propose that the fast tunneling times of loosely bound neutrons can trigger short gamma/X-ray bursts/flaring activities in magnetars and FRBs through the liberation of photons in the crust or in the star magnetic field. Beta-decay particles in the strong magnetic field move perpendicular to it in quantized Landau levels, and the electron-cyclotron energy will be equal to the electron rest-mass energy. In this scenario, these particles would also act as a seed for the high-energy electromagnetic radiation. The origin of these electromagnetic activities as well as the sources of the FRBs are unknown. Recent observations have shown a connection between these phenomena (Andersen et al. 2020; Bochenek et al. 2020; Lin et al. 2020), maybe solving the puzzling mechanism of FRBs sources.

To understand the physics of neutron tunneling times and how theoretical perturbative and nonperturbative models can be used to obtain realistic estimates, we study a one-dimensional

system where a neutron dense region has at least two similar neighbors. One-dimensional models, such as the 1D Ising model, have fundamentally impacted our knowledge of thermodynamics, critical phenomena, particle physics, conformal quantum field theories, magnetism, and emergence in many-body systems. The existence of two neighbors enhances the equilibration rates, and in three dimensions, this enhancement will increase appreciably. Because of resonant tunneling, neutrons diffuse primarily to states with approximately the same single-particle energies followed by decay to states at lower energies or by other nuclear processes such as beta-decay or gamma emission. Transfer of loosely bound neutrons and the presence of neighbors lead to neutron diffusion estimates that deviate considerably from the perturbative calculations. As expected, the neutron-neutron interaction and pairing are important effects not amenable to perturbative treatment.

2. HFB Diffusion Model

We consider the dynamics of a one-dimensional system of neutrons in a one-body potential $U(x)$ and a neutron-neutron interaction $v(x, x')$ solving the time-dependent Hartree-Fock-Bogoliubov (TDHFB) equations (Ring & Schuck 1980):

$$i\hbar \frac{\partial}{\partial t} u_\alpha(x, t) = \left\{ -\frac{\hbar^2 \Delta_x^2}{2m(\delta x)^2} + U(x) + \Gamma(x) \right\} u_\alpha(x, t) - \delta x \sum_{x'} \Delta(x, x') v_\alpha(x', t), \quad (1a)$$

$$i\hbar \frac{\partial}{\partial t} v_\alpha(x, t) = -\left\{ -\frac{\hbar^2 \Delta_x^2}{2m(\delta x)^2} + U(x) + \Gamma^*(x) \right\} v_\alpha(x, t) - \delta x \sum_{x'} \Delta^*(x, x') u_\alpha(x', t), \quad (1b)$$

where $\hbar^2/2m = 20.73 \text{ MeV fm}^2$, $|u_\alpha|^2 (|v_\alpha|^2)$ represents the probability that a pair state α is occupied (unoccupied), δx is the size step of a discretized one-dimensional mesh, and Δ_x^2 is the second-order differential operator $\Delta_x^2 \phi(x) = \phi(x + \delta x) - 2\phi(x) + \phi(x - \delta x)$. The other quantities are defined as

$$\Gamma(x) = \sum_{x'} v(x - x') \rho(x', x') \quad (2)$$

$$\Delta(x, x') = v(x - x') \kappa(x, x') \quad (3)$$

$$\rho(x, x') = \sum_{\alpha} v_\alpha^*(x, t) v_\alpha(x', t) \quad (4)$$

$$\kappa(x, x') = \sum_{\alpha} v_\alpha^*(x, t) u_\alpha(x', t), \quad (5)$$

where $\rho(x, x')$ is the density matrix, $\kappa(x, x')$ is the pairing density matrix, $\Delta(x, x')$ is the pair correlation matrix, and $\Gamma(x)$ is the interaction density. These time-dependent coupled equations are solved with a fourth-order classical Runge-Kutta method.

The initial ($t = 0$) wave function is obtained by diagonalizing the standard Hartree-Fock-Bogoliubov (HFB) equations using an expansion of single-particle states in a harmonic oscillator basis with particle-number conservation enforced with the Lagrange multiplier method (Ring & Schuck 1980). This model yields the initial states α and their energies and

Table 1

Single Particle Energy, $E_{s.p.}$, Kinetic Energy, E_{kin} , Interaction Energy, E_{int} , Pairing Energy, E_{pair} , Total Energy, E_{total} , and Neutron Separation Energy, S_n , for a System of $N = 20, 40, 80,$ and 160 Neutrons Confined in a Potential with Parameters Described in the Text

N	λ (MeV/fm $^{-2}$)	$E_{s.p.}$	E_{kin}	E_{int}	E_{pair}	E_{total}	S_n
20	2	-1353	767.9	-690.4	-6.72	-1282	1.55
40	0.1	-1830	1384	-1457	-4.97	-1908	0.96
80	1.15×10^{-2}	-1812	2222	-2550	-7.27	-2146	0.40
160	2.0×10^{-3}	-1610	3632	-4466	-12.3	-2456	0.25

Note. All energies are in units of MeV.

occupation numbers for a system of N neutrons. We assume spin symmetry, so that $u_{\alpha\uparrow} = u_{\alpha\downarrow}$ ($v_{\alpha\uparrow} = v_{\alpha\downarrow}$), which reduces the working model space to half the number of states needed.

We consider initially neutron-rich impurities of typical nuclear sizes using a confining potential $U_{t=0}(x) = U(x) + U_\lambda(x)$ with

$$U(x) = -\frac{U_0}{[1 + \exp\{|(x| - d)/a\}]}, \quad (6)$$

and parameters $U_0 = 100$ MeV, $d = 5$ fm, and $a = 1$ fm. For the neutron–neutron potential, we assume a Gaussian interaction of the form

$$v(x, x') = v_0 \exp\left(-\frac{|x - x'|^2}{2\sigma_0^2}\right), \quad (7)$$

with $v_0 = -14$ MeV and $\sigma_0 = 2.5$ fm. To simulate loosely bound neutrons and obtain the chemical potential close to the continuum, we add to $U(x)$ at $t = 0$ a confining harmonic oscillator potential $U_\lambda(x) = \lambda x^2$ and use λ as a parameter to adjust the binding energy of the system.

For $N = 20, 40, 80,$ and 160 neutrons, with $\lambda = 2, 10^{-1}, 1.15 \times 10^{-2},$ and 2×10^{-3} MeV/fm $^{-2}$, and the potential parameters for $U(x)$ and $v(x, x')$ as listed above, the solution of the static HFB equations yields valence neutrons bound by $S_n = 1.55, 0.96, 0.40,$ and 0.25 MeV for $N = 20, 40, 80,$ and 160 neutrons, respectively, where S_n denotes the neutron separation energy. This is displayed in Table 1 together with other energies in the system. The binding energies per neutron are much larger than for a regular nuclear system; however, the physics associated with the diffusion rate of the neutrons can be well understood with this model.

3. Time Evolution and Diffusion Rates

After the preparation of the initial wave function for N neutrons, we solve Equation (1) by switching off the confining potential U_λ . The potential $U(x)$ as described above is replaced by a chain of equally shaped Woods–Saxon (WS)-type potentials separated by a distance D . Namely, at $t > 0$, we make the replacement

$$U(x, d, a) \rightarrow \sum_{n=-M}^M U(x - nD, d, a). \quad (8)$$

The initial wave function, as described previously, is located at the center of the potential chain, i.e., for the term of the sum with $n = 0$. The N -neutron system is thus allowed to evolve with the neutrons tunneling through barriers with equal widths of about $D - 2(d + a)$. Equations (1a) and (1b) are solved within a box of size $L = 100$ fm and absorbing boundary conditions with an imaginary potential, located at the edges of

the box, with thickness $d_{im} = 50$ fm and strength $W_{im} = -200$ MeV. In the few cases where the box is too small, it was increased beyond $L = 100$ fm to accommodate the sequence of $2M$ WS potentials within the box. The absorbing boundary conditions avoid reflections at the borders of the box, relevant for large timescales. The number $2M$ of potential wells entering Equation (8) depends on the distance D between them. Initially, we use $M = 2-10$ for D in the range $D = 20-100$.

The N -neutron wave function is allowed to evolve and the diffusion from the dense to the uncompressed regions predominantly occurs for neutrons with the smallest separation energies. Tunneling to a neighboring region will be partially Pauli-blocked, preventing neutrons from flowing (Ogata & Bertulani 2020). Therefore, valence neutrons will move more freely between the potential pockets, and our model captures the relevant aspects of the diffusion process.

The time evolution of the neutron density enabled us to calculate the neutron diffusion speed and the net diffusion coefficient \mathcal{D} by using the equation $\partial\langle\rho\rangle/\partial t = \mathcal{D}\partial^2\langle\rho\rangle/\partial x^2$. The diffusion coefficient for the tunneling of atoms and molecules propagating in a potential lattice, created by a combination of electric, magnetic, and laser fields in an atomic trap, has been studied, e.g., in Bailey et al. (2012). The diffusion coefficient can be related to relaxation times and to thermodynamic properties of the system. Despite being a much simpler case than the one considered here, the subtle effects of quantum interference, resonant tunneling, and energy transfer to intrinsic motion render a very complicated calculation of the diffusion coefficient (Bailey et al. 2012). In our case, we consider a fermionic system that includes additional microscopic phenomena such as Pauli-blocking and pairing, increasing the degree of difficulty to calculate the diffusion, or tunneling, rate of the system. Because of that, we will adopt another calculation procedure, based on the fact that the tunneling rates are very short and amenable to a simpler approach. In our 1D model, we assess the rate at which the neutrons diffuse from a dense to an uncompressed region by calculating the neutron tunneling rate $\Lambda_n(t)$ from $\Lambda_n(t) = -dN_0/dt$, where $N_0(t)$ is the number of neutrons confined within the initial neutron-rich impurity centered at $x = 0$ corresponding to $n = 0$ in Equation (8).

Alternatively, the tunneling rate can be calculated using Gamow’s model for nuclear decay (Gamow 1928):

$$\begin{aligned} \Lambda_G &= \nu P \sim \frac{\nu}{d} \exp\left(-2 \int |\kappa(x)| dx\right) \\ &\sim \frac{\sqrt{2U_0/m}}{d} \exp\left(-\frac{2}{\hbar} \int \sqrt{2m[U(x) - E]} dx\right), \end{aligned} \quad (9)$$

where $\nu \sim v/d$ is the barrier assault frequency and $\hbar\kappa = \sqrt{2m[U(x) - E]}$ is the local momentum for a particle

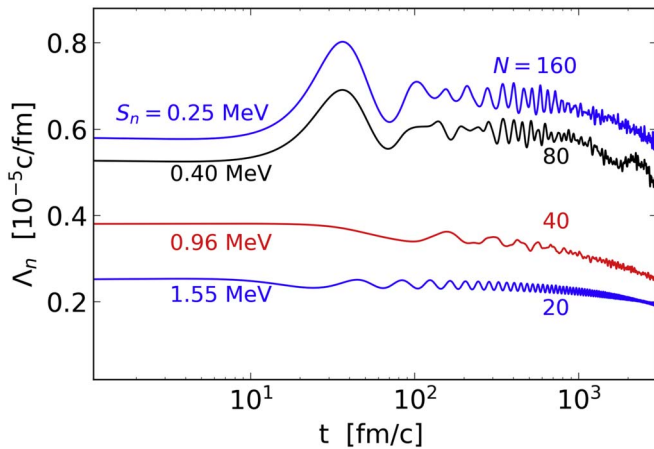


Figure 1. Neutron diffusion, or tunneling, rates as a function of time for the neutron-rich impurities separated by 20 fm with neutron numbers listed in Table 1 and a periodic row of Woods–Saxon potentials as described in the text.

with kinetic energy E . The integral is performed between the turning points where $E = U(x)$, where $U(x)$ denotes the two connected WS potentials ($n = 1$ in Equation (8)). For the most-energetic neutrons, i.e., the ones occupying the last orbital for the cases listed in Table 1, we have $v \sim \sqrt{2U_0/m}$, and the Gamow model yields increasing tunneling rates $\Lambda_G \sim (0.5\text{--}0.9) \times 10^{-5} c \text{ fm}^{-1}$ for decreasing separation energies $S_n = (1.55\text{--}0.25) \text{ MeV}$.

As shown in Figure 1, the neutron tunneling rates Λ_n calculated with the dynamical THDFB procedure, and for a relatively close region with $D = 20 \text{ fm}$, yield values that are not constant in time. Initially, the rates remain approximately constant and are overwhelmingly due to the tunneling of the most-energetic neutrons. Oscillations set in at a later stage due to wave mechanical properties such as reflections and interferences. The rates drop at some later time before they flatten out at much longer timescales when less-energetic neutrons start participating in the tunneling process. As expected, the neutron tunneling rate increases with decreasing separation energy S_n . The rates are smaller by at least an order of magnitude than those predicted by the WKB transmission model.

The smaller transmission rates calculated with the microscopic TDHFB model are partially due to the two-body interaction that makes a large contribution E_{int} to the total nuclear binding (see Table 1). An impurity is stickier due to the strong neutron–neutron interaction, and the “evaporation” or tunneling to free space regions is suppressed. From Table 1, we see that the contribution of the two-nucleon binding to the total energy reduces from 35 to 28 MeV neutron $^{-1}$ as the neutron number increases for $N = 20$ to $N = 160$. But the separation energy S_n has a stronger influence on the transfer during the initial stages due to the tunneling of valence neutrons.

To gain more insight, we switch off the two-body interaction $v(x, x')$ at $t > 0$. Figure 2 shows the average value of $\langle \Lambda_n \rangle$ for $D = 20 \text{ fm}$ during the interval $t = 0\text{--}1000 \text{ fm c}^{-1}$. The error bars represent the standard deviation of the average values. The diamonds (filled circles) are obtained by solving Equation (1) with $v(x, x') = 0$ ($v(x, x') \neq 0$). The tunneling rate increases by a factor $\simeq 4\text{--}5$ when the neutron–neutron interaction is turned off. This reinforces the need for a many-body

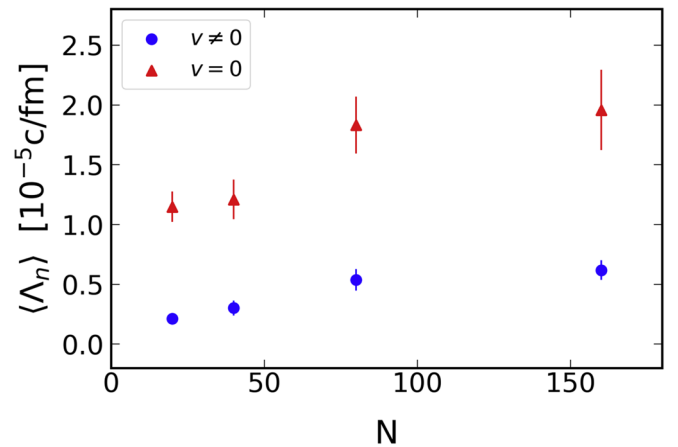


Figure 2. Average value of $\langle \Lambda_n \rangle$ for $D = 20 \text{ fm}$ during the interval $t = 0\text{--}1000 \text{ fm c}^{-1}$ for $N = 20, 40, 80,$ and 160 . The error bars represent the standard deviation of the average values. The diamonds (filled circles) are obtained by solving Equation (1) with the neutron–neutron interaction $v(x, x') = 0$ ($v(x, x') \neq 0$).

Table 2
Average Tunneling Rates $\langle \Lambda_n \rangle$ (in Units of $c \text{ fm}^{-1}$) with Increasing Separation Distances for $N = 160$ Using the Same Parameters as in Table 1 for the Initial Wave Function

D	20 fm	35 fm	50 fm	100 fm
$\langle \Lambda_n \rangle$	5.16×10^{-6}	1.13×10^{-9}	2.24×10^{-12}	4.77×10^{-24}
Λ_G	9.51×10^{-6}	1.24×10^{-8}	1.35×10^{-11}	2.93×10^{-22}

Note. The second row displays the results of the WKB method based on Equation (9).

calculation for the diffusion process when residual nucleon–nucleon interactions are relevant.

Pairing correlations are important in two neutron transfer reactions between nuclei (Broglia et al. 1968; Bes & Sorensen 1969). The enhancement of tunneling emerges in transparent analytical models for Cooper pairs and composite particles, as shown in Flambaum & Zelevinsky (2005), Bertulani et al. (2007). We study the impact of pairing switching off the pairing density matrix $\kappa(x, x')$ in TDHFB Equation (1), equivalent to solving the TD-Hartree–Fock equations. The Λ_n rates are barely changed, decreasing the tunneling rate by less than 3% for $N = 160$ and by less than 5% for $N = 20$. Therefore, there is a dominance of single-neutron tunneling in the 1D model. There is no direct correlation of this process with neutron transfer in heavy-ion exchange reactions because in the later case, there are two timescales—one for the reaction time and another for the neutron tunneling dynamics. In our model, pairing is unlikely to modify the total energy by suppressing single-neutron transfer in favor of pair transfer.

We now discuss the tunneling rate dependence on the distance between the neutron-rich impurities and the neutron gaps. The same physical properties reported above are also observed with increasing separations D . The computing time increases considerably because of exponentially smaller tunneling probabilities with increasing separation distances. This feature is displayed in Table 2 for $N = 160$ using the same parameters as in Table 1 for the initial wave function. The diffusion, or tunneling, rates obtained with the TDHFB calculations are about 2–15 times smaller than the predictions based on the Gamow model.

The tunneling rates reported here are large compared to typical ones in nuclear reactions because of the large neutron numbers and small separation energies we have adopted for the valence neutrons. Because of the Coulomb barriers and symmetry energies in normal nuclei and the large separation between them, the tunneling rates are much smaller. On the other hand, as the neutron number increases in the envelope and crust of neutron stars, the reaction rates are expected to increase accordingly when inhomogeneous conditions develop. We have also considered neutron-rich impurities with 500 and 1000 neutrons with widths and depths of the confining potentials $U(x)$ adjusted to accommodate all neutrons within the potential wells while keeping the valence neutrons at about 1 MeV binding. This time, the distance between the edges of the impurities were kept fixed at 100 fm. We obtain $\langle \Lambda_n \rangle \sim 7.23 \times 10^{-22} \text{ c fm}^{-1}$ and $\langle \Lambda_n \rangle \sim 5.14 \times 10^{-20} \text{ c fm}^{-1}$ for $N=500$ and 1000, respectively. This is in agreement with the increase of the diffusion rate with the neutron number, but it is manifestly stronger for large neutron-rich impurities. It is a probable scenario in a cataclysmic event, i.e., large neutron-rich impurities separated by large distances. If the distances become smaller due to compression waves, the neutron diffusion process can release enormous amounts of energy.

4. FRBs and Magnetars

FRBs are a new astrophysical electromagnetic phenomenon discovered in recent years. These are radio pulses with unknown origin, and the research in this field is fairly nascent. Theories to explain this phenomenon are diverse (Platts et al. 2019), ranging from highly speculative (for example, invoking alien civilizations) to more standard ones, such as the merger of compact stars (Totani 2013; Liu 2018) and fracturing crusts (Suvorov & Kokkotas 2019). The radio pulses are very bright with brief durations, typically in a range from $\sim 30 \mu\text{s}$ to $\sim 20 \text{ ms}$ (Gajjar et al. 2018; Katz 2018; Michilli et al. 2018), and apparently there is no indication of repetition for the majority of them. Relativistic particle beams with large Lorentz factors γ are possibly involved in the emission process, in a pulsar-like mechanism, where e^\pm pairs are created and accelerated to ultrarelativistic speeds in the polar cap region. Radiation coherence makes N particles radiate with N^2 times the single-particle emission (Cordes & Chatterjee 2019). In a pulsar model, the spin-down power is responsible for the electromagnetic radiated power, i.e., the loss of rotational energy of the star provides the power; therefore, an instantaneous emission cannot exceed the spin-down power in these radio emitters. However, this is possible for magnetars (SGRs/AXPs), where the radiated power is believed to come from the huge magnetic field ($B \sim 10^{12}\text{--}10^{15} \text{ G}$) instead of rotation, i.e., the decay of the ultrastrong magnetic field generates the emission. Unpredictable and unknown instabilities in these sources are responsible for bursting/flaring activities in the X-ray and gamma-ray spectrum from a few milliseconds to tens of seconds. There are three kinds of bursts: the short ones, with $\sim 10^{39}\text{--}10^{41} \text{ erg s}^{-1}$; the intermediates ones, with $\sim 10^{41}\text{--}10^{43} \text{ erg s}^{-1}$; and the giant flares, which are exceptionally rare events with energies of $\sim 10^{44}\text{--}10^{47} \text{ erg s}^{-1}$. According to the McGill (Olausen & Kaspi 2014) online catalog,¹ only 5 of 30 sources are radio emitters (in a quiescent

state), and it seems that the origin of the radio emission in these sources is different from standard radio pulsars (Turolla et al. 2015).

Recently, the possibility that FRBs have their origin in magnetars (Margalit & Metzger 2018) was raised, and there is some evidence showing that; polarization measurements suggest that FRB sources are strongly magnetized, the localization of several FRBs to star-forming regions are typical of magnetars (Bochenek et al. 2021), SGRs emit giant flares/bursts with volatility, and a more recent observation (Merghetti et al. 2020) showed that X-ray bursts from the magnetar SGR 1935+2154 were also accompanied by a very bright millisecond radio burst. Several magnetohydrodynamics instabilities can occur in few seconds (Kokkotas 2014); the lack of correlation between bursts and waiting times suggests that the trigger mechanism could be a small-scale intrinsic (nonglobal) mechanism and episodic (Suvorov & Kokkotas 2019). Li et al. (2019) showed that the waiting time ($10^{-2}\text{--}10^{-3}$) is on the order of the Alfvén crossing time,

$$t_A \sim 10^{-3} \left(\frac{\rho}{10^{13} \text{ g cm}^{-3}} \right)^{1/2} \left(\frac{L}{10^5 \text{ cm}} \right) \left(\frac{B}{10^{15} \text{ G}} \right)^{-1} \text{ s}, \quad (10)$$

where ρ is the crustal density, $L \sim R_\odot - R_c$, with R_\odot being the stellar radius and R_c the crustal radius.

It was suggested that radio emission bursts might originate from the closed field zone within the near-magnetosphere of the magnetar (Wadiasingh & Timokhin 2019), in a pulsar-like mechanism occurring near the surface of the star generated by a crust yielding event. Along the same lines, other mechanisms (Beloborodov 2017) have also considered a crustal/quake event (Petroff et al. 2019).

Here we propose that the trigger for the short gamma-/X-ray bursts and FRBs could be the diffusion of neutrons in an inhomogeneous density environment in the crust. The diffusion can occur in a short time in a region at the crust where neutron-rich nuclei or neutron-rich impurities donate neutrons to a neighborhood poor in neutron content, generating beta-decay or gamma emission and thus releasing a large amount of energy. It should be stressed that the formation of neutron-rich regions with the described properties is a basic assumption of our model. The electron from the beta decay is relativistic in the regions where the density is $> 10^6 \text{ g cm}^{-3}$ and will act as seeds for the high-energy emission and coherent emission which lead to a brief radio emission. These electrons come out from the crust to the inner magnetosphere and will give rise to an e^\pm cascade, producing high-energy radiation via synchrotron or inverse Compton scattering. These mechanisms will drive Alfvén waves, and as shown in Kumar & Bošnjak (2020), a large-amplitude Alfvén wave packet can possibly be launched by a disturbance in the near-surface of the magnetar and part of the wave energy is converted to coherent radio emission in a few tens of the neutron star radii. In our proposed mechanism, as the magnetic structures evolve in a neutron star, the magnetic field flux tubes passing from the core to the crust build up a large stress (Ruderman et al. 1998). This happens for years until the shear strain reaches a critical value $s_{\text{cr}} \approx 0.1$ in the lattice (Horowitz & Kadau 2009). By exceeding this value, plastic failures are triggered according to molecular dynamics simulations (Horowitz & Kadau 2009; Chugunov & Horowitz 2010). These deformations will give rise to the manifestation of a rapidly acting hydrodynamics instability (Thompson & Duncan 1996; Rheinhardt & Geppert 2002),

¹ <http://www.physics.mcgill.ca/~pulsar/magnetar/main.html>

leading to the emergence of large amplitudes, compressing waves, part of whose energy is promptly dissipated and converted into radiation, and part stored in highly compressed waves. The fate of the energy carried by those waves is not well known or how they are damped. We propose that this energy is responsible for forming inhomogeneous neutron distributions. As the wave propagates in the crust with a velocity $v \sim 10^{-2}c$ (Li & Beloborodov 2015), it interacts with the solid lattice, donating energy to it, becoming damped in the process, changing the local density, and forming the neutron-rich impurities that are quickly relaxed by neutron tunneling, e.g., see the lower panel of Figure 2 of Horowitz & Kadau (2009), where the plastic deformations are shown in red, i.e., where the ion lattice suffers deviations from the ideally uniformly sheared bbc lattice. We assume that those red regions are the places where the local changes in the density occur, leading to the formation of neutron-rich regions, at close distances L , together with neighborhoods of poor neutron content, which can accept neutrons, thus leading to quick relaxation by neutron tunneling. According to our estimates, the tunneling process can suddenly release energy and trigger the burst/flaring in SGRs/AXPs and FRBs. The tunneling process effectively takes no time, and the duration of the burst is related to the time when the wave crosses the crust. Changes in neutron density could also lead to pressure perturbations $\Delta P \sim n_e \Delta \mu$, where $\Delta \mu = \mu_e + \mu_p + \mu_n$, i.e., the pressure gradient is related to the chemical potentials. The pressure gradient leads to perturbations in the magnetic field, and through ambipolar diffusion, it heats up the crust (Beloborodov & Li 2016).

To provide a crude estimate of the total energy released in a burst, E_{burst} , we assume that on average, the separation energy of the valence neutrons is $\epsilon \sim 1$ MeV and the ensuing tunneling to a neighboring site releases a similar amount of energy. We assume that

$$\begin{aligned}
 E_{\text{burst}} &= \int \epsilon N_{\text{imp}} (1 - e^{-\Lambda_G t}) dt \sim \epsilon N_{\text{cl}} \Lambda_G \Delta t \\
 &\sim \frac{\epsilon N_{\text{cl}} 10^2 L}{\alpha D} \sqrt{\frac{2U_0}{mc^2}} \exp\left(-\frac{2D\sqrt{2mc^2\epsilon}}{\hbar c}\right), \quad (11)
 \end{aligned}$$

where Λ_G is the tunneling rate from Equation (9). The time during which the tunneling process is effective as the wave sweeps through the crust is given by $\Delta t \approx L/v = 10^2 L/c$, with $L \approx 2$ km being the approximate distance that the wave propagates and dampens by formation of neutron-rich impurities, and N_{imp} is the number of impurities involved in the process. We further assume that the impurities have a dimension αD , where $\alpha > 1$ takes into account large impurity sizes. Notice that the separation distance D now represents the distance between the edges of the neutron-rich impurities. In Equation (11), we have assumed that $\Lambda_G \Delta t \ll 1$. From the numbers presented in Table 2, this is likely the case for $D \gtrsim 50$ fm. At smaller distances, the tunneling rates are so large that $\Lambda_G \Delta t \gg 1$ and a better estimate is $E_{\text{burst}} \sim \epsilon N_{\text{cl}}$. We will use the approximation on the right-hand side of Equation (11) as a basis for our predictions.

To determine the number of impurities involved in a rapid emission, we consider the polar cap region, which can be estimated through the cylindrical region of radius R_L encapsulating the closed magnetic field lines. The maximum velocity of the particles within this region will be the speed of light, so that $c = \Omega R_L$, with Ω being the star's rotational angular

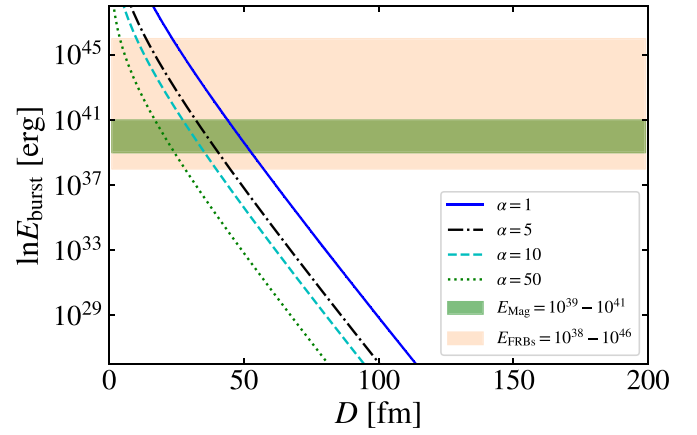


Figure 3. Energy burst as a function of the separation distance D for $\alpha = 1, 5, 10, 50$. The green shaded horizontal region represents the observed values of short burst in magnetars, while the orange represents the observed values of FRBs.

frequency. In the particle emission region, the lines are open and the boundaries define the polar cap with a radius, in the dipole field, given by $R_p = R \sin \theta_p = R \sqrt{R/R_L} = R \sqrt{\Omega R/c}$, where R is the star radius (see, e.g., Ghosh 2007). Therefore, the polar cap radius will depend on the period $P = 2\pi/\Omega$ (for magnetars, 2–12 s) and the star radius R . Considering a neutron star with $R = 11$ km, then $R_p \approx 118$ m and 48 m for $P = 2$ s and 12 s, respectively. The polar cap in a twisted magnetic field configuration

is $R_p = R \sin \theta_p = R \sqrt{(R\Omega/c)^n / (15 + 17n)/32}$, where n evolves from $n < 1$ to $n = 1$. Twisted field lines may enhance the polar cap radius in magnetars to about 1 or 2 km (Tong 2019). We can estimate the height under the polar cap, h_{ρ_0} , from the star surface to the layer of density $\rho = \rho_0$, where ρ_0 is the nuclear matter saturation density, yielding $h_{\rho_0} \approx 2$ km. The crust is composed of the outer and inner crusts: The first one extends from the atmosphere bottom to the layer of density $\rho_{\text{ND}} = 4 \times 10^{11} \text{ g cm}^{-3}$ with some hundred meters; the second one is about 1 km and the density goes from ρ_{ND} to $0.5\rho_0$, so one can estimate that the thickness of the crust is about 1–2 km (Haensel et al. 2007). The volume of interest for the emission region in magnetars is $V = \pi R_p^2 h_{\rho_0}$. The number of impurities in this region is

$$N_{\text{imp}} = \frac{V}{4/3\pi(\alpha D)^3} \sim \frac{3R^2 h_{\rho_0}}{4\alpha^3 D^3} \frac{(R\Omega/c)^n}{(15 + 17n)/32}. \quad (12)$$

We consider three scenarios with $\alpha = 1, 5, 10, 50$, taking into account neutron-rich impurities that can also be much larger than the distance between them. In Figure 3, we show the energy emitted in a burst as a function of their separation distance D , considering a polar cap radius $R_p = 2$ km. The green shaded horizontal region displays the observed values of short bursts in magnetars $\sim 10^{39} - 10^{41} \text{ erg s}^{-1}$ (Turolla et al. 2015) and the shaded orange, the values of FRBs $\sim 10^{38} - 10^{46} \text{ erg s}^{-1}$ (Zhang 2020).

Figure 3 also shows that the bursts can become comparable with the observed values of short burst in magnetars, and the observed values of FRBs, if the dense neutron sites are within distances of $D \sim 50$ fm or lower. These are rough estimates based on the WKB approximation with possible corrections by at least an order of magnitude. As we have discussed previously, a microscopic calculation can change these results

appreciably if carried out within a proper three-dimensional lattice which offers more tunneling opportunities. One also sees from the figure that smaller impurities favor larger energy yields. This feature is likely to remain as a robust result in more detailed microscopic calculations.

5. Conclusions

We have developed a microscopic TDHFB model to describe neutron diffusion rates due to tunneling from neutron-rich impurities to regions void of neutrons. The model is 1D but displays many features of the time-dependent behavior of strong interacting particles.



Our main findings in this study include, but are not limited to the following: (a) there are marked differences between estimates based on WKB models and the time-dependent microscopic modeling for the detachment and diffusion of neutrons in an inhomogeneous neutron environment. (b) Tunneling is smaller than those obtained with perturbative (i.e., WKB) predictions, but this could change in three-dimensional calculations. (c) The role of pairing is subtle and might strongly depend on the system being studied.

Time-dependent microscopic calculations show that the subjects of density homogenization and isospin diffusion in nuclear reactions and in stellar environments deserve more extensive studies. Perturbative estimates are likely to yield poor results because of the microscopic properties of strongly interacting systems, such as the different contributions of the interactions to the total energy and the related energy rearrangement due to tunneling. Microscopic calculations are rich in physics details and are now becoming feasible for 3D calculations, e.g., Stetcu et al. (2015), though with the shortcoming of costly computation time even with supercomputers. It is worth mentioning that neutron tunneling has been considered in previous works in the context of diffusion of unbound neutrons in the inner crust (Bisnovaty-Kogan & Chechetkin 1979) and between nuclei in transiently accreting neutron stars (Chugunov 2018, 2019).

Nonperturbative calculations of neutron tunneling rates in inhomogeneous neutron distributions may play an important role in many astrophysics scenarios including rare events involving neutron stars. As proposed in this work, sudden medium modifications in cataclysmic environments, such as supernovae, neutron star mergers, or the creation of energy stored in inhomogeneous regions in the crust of neutron stars due to compression waves from a star quake, can all lead to gamma or radio bursts when proper conditions for neutron diffusion is attained. We conclude from our analysis that many-body nuclear physics dictates that such conditions depend on the existence of inhomogeneous neutron distributions, i.e., neutron-rich impurities separated by relatively small distances.

We have benefited from useful discussions with Sanjay Reddy and Takashi Nakatsukasa. This work has been supported in part by the US DOE grant No. DE-FG02-08ER41533.

ORCID iDs

Carlos A. Bertulani  <https://orcid.org/0000-0002-4065-6237>
Ronaldo V. Lobato  <https://orcid.org/0000-0001-5755-5363>

References

- Andersen, B. C., Bandura, K. M., Bhardwaj, M., et al. 2020, *Natur*, 587, 54
Bailey, T., Bertulani, C. A., & Timmermans, E. 2012, *PhRvA*, 85, 033627
Baym, G., Hatsuda, T., Kojo, T., et al. 2018, *RPPh*, 81, 056902
Baym, G., & Pethick, C. 1979, *ARA&A*, 17, 415
Beloborodov, A. M. 2017, *ApJL*, 843, L26
Beloborodov, A. M., & Li, X. 2016, *ApJ*, 833, 261
Bertulani, C., & Piekarewicz, J. 2012, Neutron Star Crust, Space Science, Exploration and Policies Series (Hauppauge, NY: NOVA Science Publishers)
Bertulani, C. A., Flambaum, V. V., & Zelevinsky, V. G. 2007, *JPhG*, 34, 2289
Bes, D. R., & Sorensen, R. A. 1969, The Pairing-Plus-Quadrupole Model (New York: Springer US), 129
Bisnovaty-Kogan, G. S., & Chechetkin, V. M. 1979, *PhyU*, 22, 89
Blaes, O., Blandford, R., Goldreich, P., & Madau, P. 1989, *ApJ*, 343, 839
Blaschke, D., Glendenning, N., & Sedrakian, A. 2008, Physics of Neutron Star Interiors (Berlin: Springer)
Bochenek, C. D., Ravi, V., Belov, K. V., et al. 2020, *Natur*, 587, 59
Bochenek, C. D., Ravi, V., & Dong, D. 2021, *ApJL*, 907, L31
Broglia, R. A., Riedel, C., & Soerensen, B. 1968, *NuPhA*, 107, 1
Chamel, N. 2013, *PhRvL*, 110, 011101
Chamel, N., & Haensel, P. 2008, *LRR*, 11, 10
Chugunov, A. I. 2018, *MNRAS Lett.*, 483, L47
Chugunov, A. I. 2019, *MNRAS Lett.*, 483, L47
Chugunov, A. I., & Horowitz, C. J. 2010, *MNRAS Lett.*, 407, L54
Cordes, J. M., & Chatterjee, S. 2019, *ARA&A*, 57, 417
De Blasio, F. V., & Lazzari, G. 1998, *NuPhA*, 633, 391
Flambaum, V. V., & Zelevinsky, V. G. 2005, *JPhG*, 31, 355
Fryer, C. L., Herwig, F., Hungerford, A., & Timmes, F. X. 2006, *ApJL*, 646, L131
Gajjar, V., Siemion, A. P. V., Price, D. C., et al. 2018, *ApJ*, 863, 2
Gamow, G. 1928, *ZPhy*, 51, 204
Ghosh, P. 2007, Rotation and Accretion Powered Pulsars (Singapore: World Scientific)
Haensel, P., Potekhin, A. Y., & Yakovlev, D. G. 2007, Neutron Stars 1: Equation of State and Structure (New York: Springer)
Heiselberg, H., & Pandharipande, V. 2000, *ARNPS*, 50, 481
Horowitz, C. J., & Kadau, K. 2009, *PhRvL*, 102, 191102
Huppenkothen, D., D'Angelo, C., Watts, A. L., et al. 2014, *ApJ*, 787, 128
Katz, J. I. 2018, *PtPNP*, 103, 1
Kobyakov, D., & Pethick, C. J. 2014, *PhRvL*, 112, 112504
Kokkotas, K. D. 2014, in AIP Conf. Proc. 1577: V Leopoldo García-Colín Mexican Meeting on Mathematical and Experimental Physics (Melville, NY: AIP), 119
Kondratyev, V. N. 2002, *PhRvL*, 88, 221101
Kumar, P., & Bošnjak, Ž. 2020, *MNRAS*, 494, 2385
Lattimer, J., & Prakash, M. 2004, *Sci*, 304, 536
Li, B., Li, L.-B., Zhang, Z.-B., et al. 2019, *IJCAA*, 1, 22
Li, X., & Beloborodov, A. M. 2015, *ApJ*, 815, 25
Lin, L., Zhang, C. F., Wang, P., et al. 2020, *Natur*, 587, 63
Liu, X. 2018, *Ap&SS*, 363, 242
Margalit, B., & Metzger, B. D. 2018, *ApJL*, 868, L4
Mereghetti, S., Savchenko, V., Ferrigno, C., et al. 2020, *ApJL*, 898, L29
Metzger, B. D., Beniamini, P., & Giannios, D. 2018, *ApJ*, 857, 95
Michilli, D., Seymour, A., Hessels, J. W. T., et al. 2018, *Natur*, 553, 182
Ogata, K., & Bertulani, C. A. 2020, *JPhG*, 47, 095101
Olausen, S. A., & Kaspi, V. M. 2014, *ApJS*, 212, 6
Oyamatsu, K., & Iida, K. 2007, *PhRvC*, 75, 015801
Pacini, F., & Ruderman, M. 1974, *Natur*, 251, 399
Petroff, E., Hessels, J. W. T., & Lorimer, D. R. 2019, *A&ARv*, 27, 4
Piekarewicz, J., & Sánchez, G. T. 2012, *PhRvC*, 85, 015807
Piro, A. L., & Ott, C. D. 2011, *ApJ*, 736, 108
Platts, E., Weltman, A., Walters, A., et al. 2019, *PhR*, 821, 1
Ravenhall, D. G., Pethick, C. J., & Wilson, J. R. 1983, *PhRvL*, 50, 2066
Rheinhardt, M., & Geppert, U. 2002, *PhRvL*, 88, 101103
Ring, P., & Schuck, P. 1980, The Nuclear Many-body Problem (New York: Springer)
Ruderman, M., Zhu, T., & Chen, K. 1998, *ApJ*, 492, 267
Saakyan, G. S., & Sedrakyan, D. M. 1972, *Ap*, 8, 170
Stetcu, I., Bertulani, C. A., Bulgac, A., Magierski, P., & Roche, K. J. 2015, *PhRvL*, 114, 012701
Suvorov, A. G., & Kokkotas, K. D. 2019, *MNRAS*, 488, 5887
Thompson, C., & Duncan, R. C. 1996, *ApJ*, 473, 322
Tong, H. 2019, *MNRAS*, 489, 3769
Totani, T. 2013, *PASJ*, 65, L12
Troja, E., Rosswog, S., & Gehrels, N. 2010, *ApJ*, 723, 1711

Tsang, D., Read, J. S., Hinderer, T., Piro, A. L., & Bondarescu, R. 2012, [PhRvL](#), **108**, 011102
Turolla, R., Zane, S., & Watts, A. L. 2015, [RPPh](#), **78**, 116901

Wadiasingh, Z., & Timokhin, A. 2019, [ApJ](#), **879**, 4
Zhang, B. 2020, [Natur](#), **587**, 45